Reversible Film Formation From PS Doped PNIPAM Particles in Various Compositions

Ş. Uğur,[1] Ö. Yargi,[1] Ö. Pekcan[2]
[1]*Department of Physics, Istanbul Technical University, 34469 Maslak, Istanbul, Turkey*

[2]*Department of Physics, Işik University, Maslak, 34398 Istanbul, Turkey*

Film formation from polystyrene (PS) doped poly(*N*-isopropylacrylamide) (PNIPAM) particles was studied using photon transmission technique. The transmitted light intensity, I_{tr}, was monitored during film formation process. Films were prepared by mixing PS and PNIPAM particles in various compositions ranging from 5 to 50 %. Samples were separately heated and cooled in constant rate at temperatures ranging from 10 to 100°C. The increase and decrease in I_{tr} during heating–cooling cycles were explained by void closure and void reconstruction processes. The corresponding activation energies were measured during the reversible film formation process. Percolation model was used to interpret the distribution of PS particles in PNIPAM lattice. POLYM. COMPOS., 29:179–186, 2008. © 2007 Society of Plastics Engineers

INTRODUCTION

Poly(*N*-isopropylacrylamide) (PNIPAM) particles are known as cross-linked colloidal particles that are swollen in a good solvent and exhibit behavior ranging from that of polymer solutions to that of hard spheres [1–4]. Since the interaction forces between PNIPAM particles can be controlled by charges on the particles and solvent quality, these dispersions have been used as model systems for the study of phase transitions. PNIPAM particles that swell in water have been used for automotive surface coating and controlled drug delivery [5, 6].

PNIPAM dispersion was first synthesized using surfactant-free precipitation polymerization [7]. Similar to the behavior of the PNIPAM macrogel, the PNIPAM microgel particles swell in water at room temperature but shrink and undergo a reversible volume phase transition at around 34°C [8]. Because of its size, the microgel responds to environmental stimuli much faster than does the macrogel. The volume phase transition of the PNIPAM microgel has been studied and compared with that of bulk gels and linear polymers using light-scattering and small-angle neutron scattering techniques [9, 10]. Rheological properties of the PNIPAM dispersion have been investigated [16, 17]. The viscosity of the PNIPAM microgel dispersion can be changed by 2 orders of magnitude by temperature-induced swelling of the particles. The monodispersed PNIPAM microgel particles can form colloidal crystals and glasses in concentrated dispersions [11, 12]. The crystal structure of this material has been identified using small-angle neutron scattering techniques [13]. The crystal can be processed in its disordered state, and it can be reformed to its crystal state upon cooling [14]. On the other hand, ionized PNIPAM dispersion can be electrostatically stabilized, and they form colloidal crystal arrays at low polymer content [15]. Such an array has potential applications in sensors technology.

Latex films are generally formed by coalescence of submicron polymer particles in the form of a colloidal dispersion, usually in water. The term "latex film" normally refers to a film formed from soft latex particles (T_g below room temperature) in which the forces accompanying the evaporation of water are sufficient to compress and deform the particles into transparent, void-free film. However, latex films can also be obtained by compression molding of a film of dried latex powder composed of relatively hard polymers, such as polystyrene (PS) or poly(methyl methacrylate) (PMMA) that has T_g above room temperature. Aqueous dispersion of soft latex particles are called low-T_g, while nonaqueous dispersion of hard polymer particles are generally referred to as high-T_g. High-T_g latex particles remain essentially discrete and undeformed during drying. The mechanical properties of such films can be evolved after all the solvent has evaporated by annealing process, which first leads to void closure and then interdiffusion of chains across particle–particle boundaries. Film formation from high- and low-T_g particles can occur in several stages. In both cases, the first stage corresponds to the wet initial state. Evaporation of solvent leads to second stage in which the particles form a close packed array. If the par-

Correspondence to: Ö. Pekcan; e-mail: pekcan@isiskun.edu.tr
DOI 10.1002/pc.20378
Published online in Wiley InterScience (www.interscience.wiley.com).
© 2007 Society of Plastics Engineers

WILEY InterScience® DISCOVER SOMETHING GREAT

ticles are soft, they are deformed to polyhedrons. Hard latex, however, stay undeformed at this stage. Annealing of soft particles causes diffusion across particle–particle boundaries, which leads the film to a homogeneous continuous material. Annealing of hard latex systems first leads deformation of particles to void closure [16, 17] and then, after the voids disappear, diffusion across particle–particle boundaries starts.

Small-angle neutron scattering (SANS) method was used to study latex film formation at molecular level by Sperling and coworkers on compression-molded PS film [18]. Direct-nonradiative energy transfer (DET) method was used to investigate the film formation process from dye-labeled polymeric particles [19–21]. Steady state fluorescence technique combined with DET was used to examine healing and interdiffusion processes in the dye-labeled PMMA latex systems [22, 23]. Photon transmission method has been performed to study latex film formation from PMMA and PS particles, using the UV–vis (UV) technique as a function temperature and time [24–26].

In this work, film formation from PS-doped PNIPAM particles was studied using photon transmission technique. Films were prepared by mixing PS with PNIPAM particles in various compositions. The mixtures then were heated and cooled to room temperature to observe film formation process. The transmitted light intensity, I_{tr}, was monitored during heating–cooling cycles. The increase and decrease in I_{tr} during these cycles were explained by void closure and void reconstruction processes. The corresponding activation energies were measured. Percolation model was used to study the distribution of PS particles in PNIPAM lattice.

EXPERIMENTAL

PS Preparation

PS particles were produced via surfactant-free emulsion polymerization process. The polymerization was performed batch-wise, using a thermostatted reactor equipped with a condenser, thermocouple, mechanical stirring paddle, and nitrogen inlet. The agitation rate was 400 rpm and the polymerization temperature was controlled at 70°C. Water (100 ml) and styrene (5 g) were first mixed in the polymerization reactor and the temperature was kept constant (at 70°C). Potassium peroxodisulfate (KPS) initiator (0.1 g) dissolved in small amount of water (2 ml) was then introduced in order to induce styrene polymerization. SDS (2.5 g/ml) was added in the polymerization recipe to reduce the particle size. The polymerization was conducted for 18 hours. Here it has to be mentioned that pyrenes are exclusively labeled near the surface of the particles. The produced PS particles are fairly monodisperse, all having very similar mean diameters (900 nm).

PNIPAM Preparation

Fluorescent PNIPAM microgel particles were synthesized via precipitation polymerization process. NIPAM from Kodak was purified using a 60/40 (v/v) of hexane and toluene mixtures. Methylene bisacrylamide (MBA) from Aldrich was used as crosslinker monomer and was used as received. Fluorescent monomer 1-pyrenylmethacrylate (PolyFluorTM 394) was from Polysciences, Inc., and was used as received.

The polymerization was performed using NIPAM (1.2 g), MBA (0.059 g), and KPS (0.018 g) as initiator. The recipe established by Menuier et al. [27, 28] was slightly modified by introducing 1-pyrenylmethacrylate as a fluorescence compound (0.0054 g). All the reactants were first solubilized in water and introduced in the polymerization reactor. The polymerization was conducted (in 50 ml deionised water) under nitrogen atmosphere and at 70°C. The polymerization reaction was carried out in 100 ml four-necked glass reactor equipped with a glass anchor-type agitator (200 rpm), condenser, and nitrogen inlet. The polymerization reaction was conducted for 16 h. The final conversion was gravimetrically determined and found to be 98.5%. The mean diameter of synthesized PNIPAM particles was 320 nm.

Film Preparation

Nine different films were prepared from the mixture of PNIPAM and PS dispersion by placing the same number of drops on a glass plates with the size of 0.8 × 2.5 cm^2 and allowing the water to evaporate. $\frac{PS}{PS+PNIPAM}$ ratios in these films were chosen as 0, 5, 10, 15, 20, 25, 30, 40, 50 wt %. Then samples were separately heated and cooled at 2.3°C/min rate at temperatures ranging from 10 to 100°C. The temperature was maintained within 0.1°C for 20–40°C, and 1°C for 40–100°C during annealing. Figure 1 presents the atomic force micrograph (AFM) of 20 wt % PS-doped PNIPAM film.

UV Measurements

Photon transmission experiments were carried out using model DU 530 Life Science UV spectrometer from

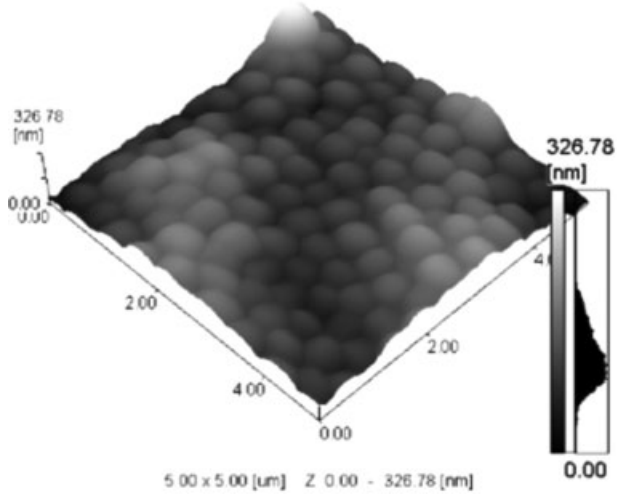


FIG. 1. AFM image of the PNIPAM film doped with 20 wt % PS.

DOI 10.1002/pc

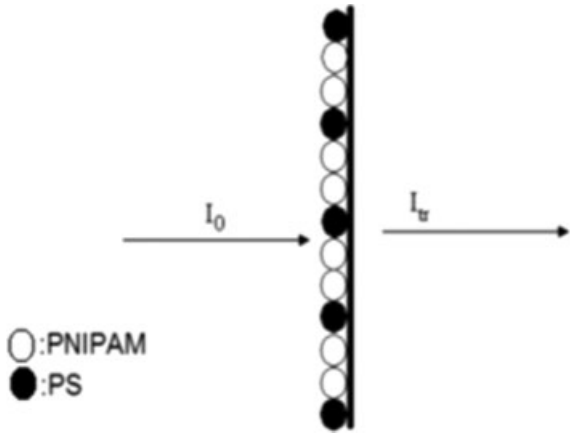


FIG. 2. The position of the film in UV spectrometer. I_0 and I_{tr} are the incident and transmitted light intensities, respectively.

Beckman. The transmittances of the films were detected at 400 nm. A glass plate was used as a standard for all UV experiments. In situ measurements were carried out at different heating and cooling rates. The sample position and the transmitted light intensity, I_{tr}, are presented in Fig. 2. AFM images were obtained by using SPM-9500-J3 Shimadzu scanning probe microscopy.

THEORETICAL CONSIDERATIONS

Percolation

Initially the percolation theory has been associated with a paper of Broadbent and Hammersley, which discussed the general situation of a fluid spreading randomly through a medium [29]. The most interesting feature of percolation phenomenon is the existence of a percolation threshold, p_c, below which spreading process is confined to be a finite region. The spread of a blight from tree to tree in an orchard was discussed by Broadbent and Hammersley, in which the trees are planted on intersection of a square lattice. The percolation threshold, p_c, for this problem is around 0.6 for so-called "site percolation" on a square lattice. The other example is the seepage of water in the cracks and fractures of a rock formation. A similar problem for practical interest is the spread of water displacing oil in porous rocks, where neighboring pores are connected by small capillary channels [30]. If no oil in the system injected water into any given pore, it may only invade another pore through capillary channels or "bonds." The pores are "sites" connected to the chosen centre of injection form what is called a "cluster." The largest cluster spans the lattice connecting the left and right edges to the bottom edge, which is called "percolating cluster." The percolation probability, $p_\infty(p)$, is defined as the probability that water injected at a site, chosen at random, will wet infinitely many pores. Here one has to notice that the probability for having a pore at all the sites where water injection is attempted is p. Extensive simulations and theoretical work have shown that the percolation probability vanishes as a power-law tends to p_c.

$$p_\infty(p) \approx (p - p_c)^\beta \quad \text{for } p > p_c \text{ and } p \to p_c \tag{1}$$

In a simple cubic lattice, p_c is found to be 0.31 for site percolation and 0.249 for bond percolation models [31]. The exponent β for a simple cubic lattice is 0.45, for percolation model, however, β is very close to 1.0 in classical model [31].

Voids Closure

Latex deformation and void closure between particles can be induced by shearing stress, which is generated by surface tension of polymer, i.e., polymer–air interfacial tension. The void closure kinetics can determine the time for optical transparency and latex film formation [32]. In order to relate the shrinkage of spherical void of radius, r, to the viscosity of surrounding medium, η, an expression was derived and given by the following relation [32]:

$$\frac{dr}{dt} = -\frac{\gamma}{2\eta}\left(\frac{1}{\rho(r)}\right) \tag{2}$$

where γ is surface energy, t is time, and $\rho(r)$ is the relative density. It has to be noted that here surface energy causes a decrease in void size and the term $\rho(r)$ varies with the microstructural characteristics of the material, such as the number of voids, the initial particle size, and packing. *Equation 2* is similar to *1*, which was used to explain the time dependence of the minimum film formation temperature during latex film formation [33]. If the viscosity is constant in time, integration of *Eq. 2* gives the relation as

$$t = -\frac{2\eta}{\gamma}\int_{r_0}^{r} \rho(r)\, dr \tag{3}$$

where r_0 is the initial void radius at time $t = 0$.

The dependence of the viscosity of polymer melt on temperature is affected by the overcoming of the forces of macromolecular interaction which enables the segments of polymer chain to jump over from one equilibration position to another. This process happens at temperatures at which free volume becomes large enough and is connected with the overcoming of the potential barrier. Frenkel–Eyring theory produces the following relation for the temperature dependence of viscosity [34–36].

$$\eta = (N_0 h/V)\exp(\Delta G/kT) \tag{4}$$

where N_0 is Avagadro's number, h is Planck's constant, V is molar volume, and k is Boltzmann constant. It is known that $\Delta G = \Delta H - T\Delta S$, then *Eq. 4* can be written as

$$\eta = A\exp(\Delta H/kT) \tag{5}$$

where ΔH is the activation energy of viscous flow, i.e., the amount of heat which must be given to 1 mol of ma-

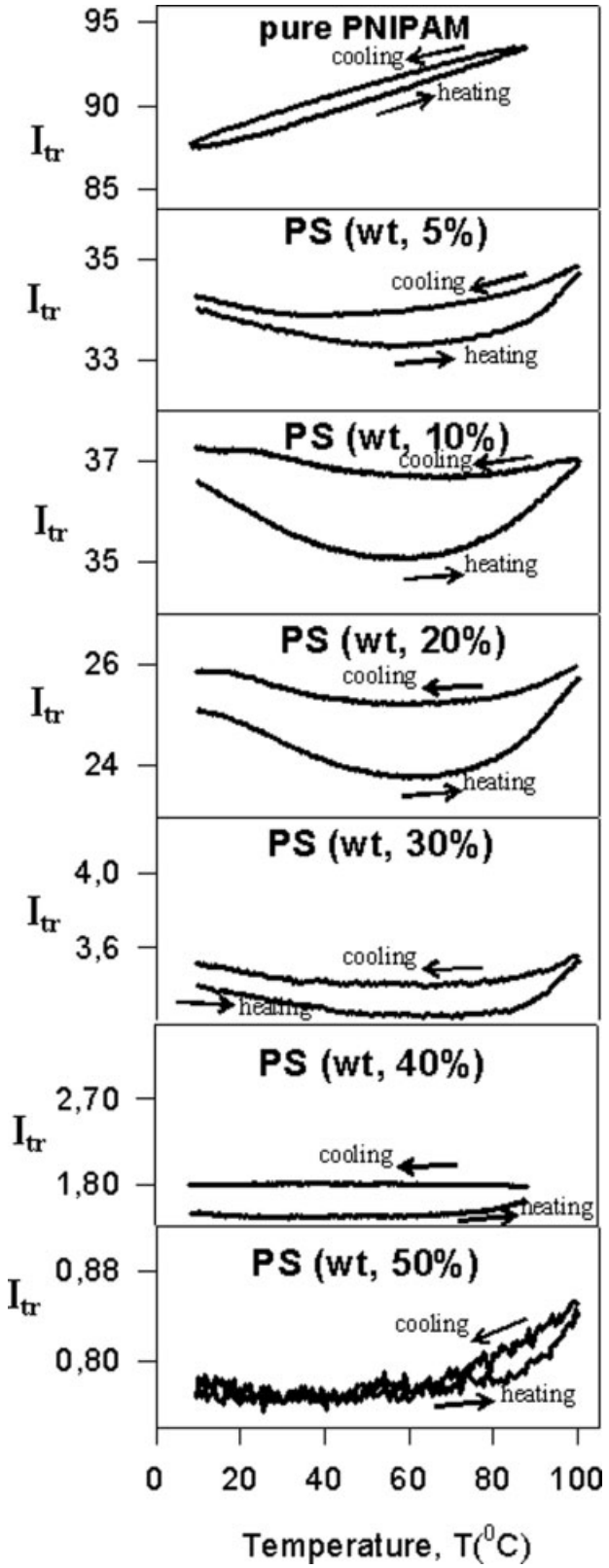


FIG. 3. Transmitted light intensity, I_{tr} versus temperature, T curves for PS-doped PNIPAM films in various compositions. Arrows present cooling and heating cycles, respectively.

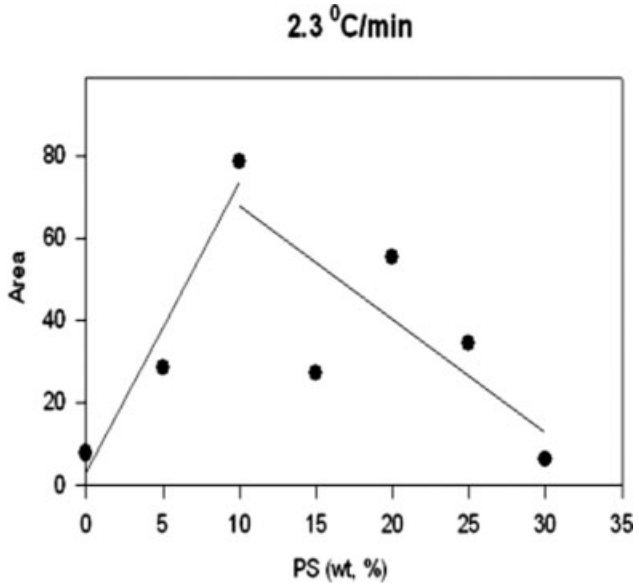


FIG. 4. Plot of the areas under hysteresis curves versus PS content in wt %.

terial for creating the act of a jump during viscous flow. ΔS is the entropy of activation of viscous flow. Here A represents a constant for the related parameters that do not depend on temperature. Combining *Eqs. 3* and *5*, the following useful equation is obtained:

$$t = -\frac{2A}{\gamma}\exp\left(\frac{\Delta H}{kT}\right)\int_{r_0}^{r}\rho(r)\,dr \tag{6}$$

In order to quantify the above results, *Eq. 6* can be used by assuming that the interparticle voids are of equal size and number of voids stay constant during film formation (i.e. $\rho(r)\propto r^{-3}$), then integration of *Eq. 6* gives the relation:

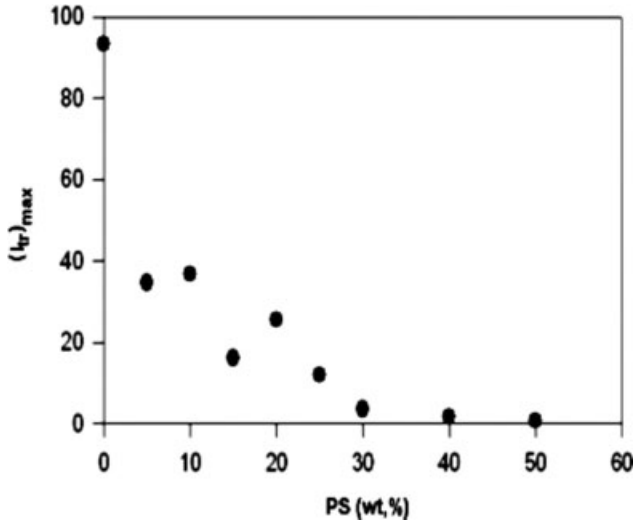


FIG. 5. Plot of $(I_{tr})_m$ versus PS content in wt %.

DOI 10.1002/pc

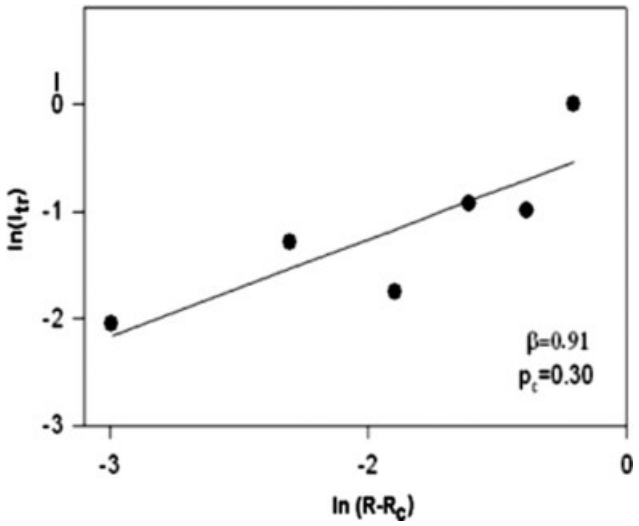


FIG. 6. Log–log plot of the data in Fig. 5. The slope of the straight line produced the critical exponent β in *Eq. 1*.

$$t = \frac{2AC}{\gamma}\exp\left(\frac{\Delta H}{kT}\right)\left(\frac{1}{r^2} - \frac{1}{r_0^2}\right) \tag{7}$$

where C is a constant related to relative density $\rho(r)$.

RESULTS AND DISCUSSION

Figure 3 compares transmitted light intensity, I_{tr}, versus temperature, T, curves of various PS-doped PNIPAM films at 2.3°C/min cooling–heating rate. All curves present hysteresis by predicting a reversible film formation process. Except pure PNIPAM film, all others show minima in heating and cooling cycles. It is seen in Fig. 3 that inclusion of PS into PNIPAM lattice strongly decreases the transmitted light intensity. Hysteresis loops of I_{tr} upon heating and cooling present at different areas. Areas under the hysteresis curves for different PS content are plotted in Fig. 4. It is interesting to note that maximum area has occurred for 10 wt % PS-doped film. On the other hand,

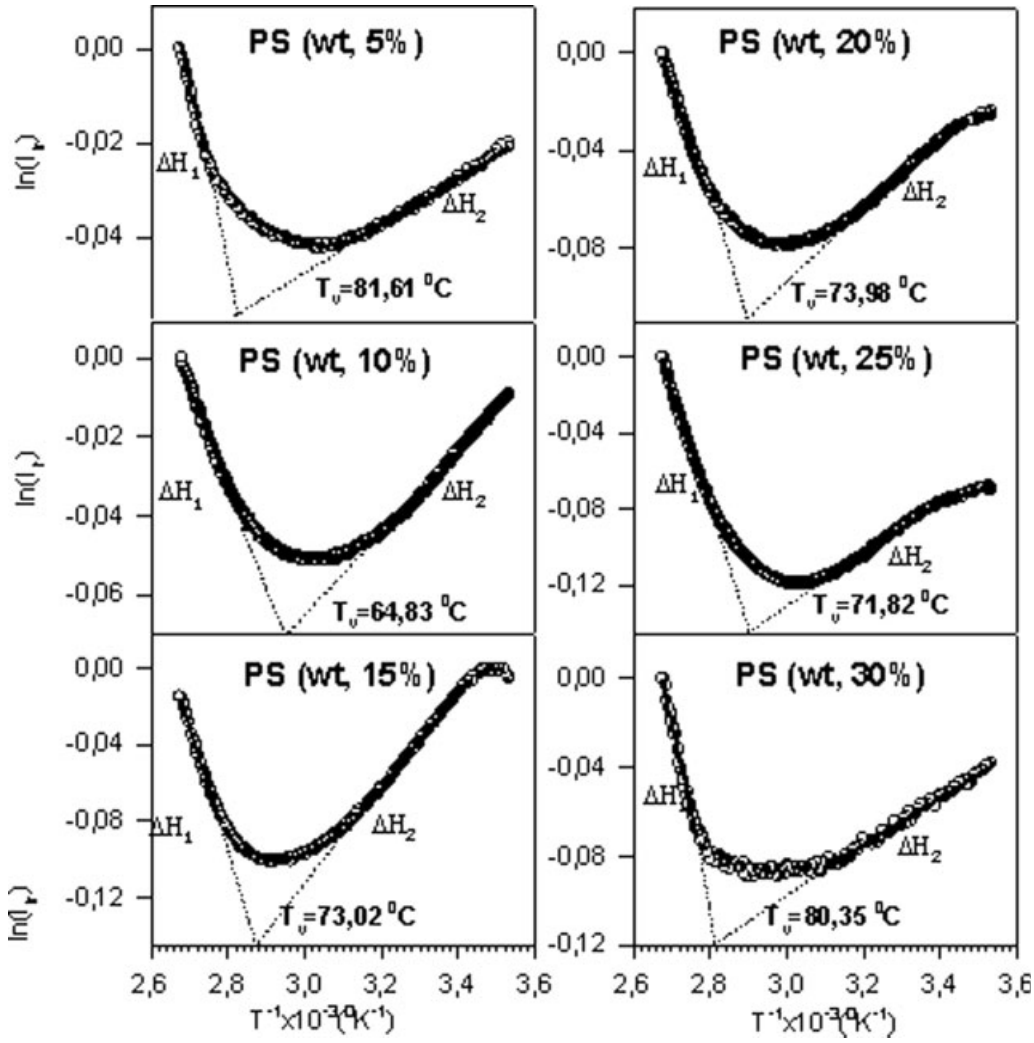


FIG. 7. Plots of ln I_{tr} versus T^{-1} curves and their fits to *Eq. 12* for heating process. The slopes of straight lines produced void closure activation energies (ΔH_1 and ΔH_2).

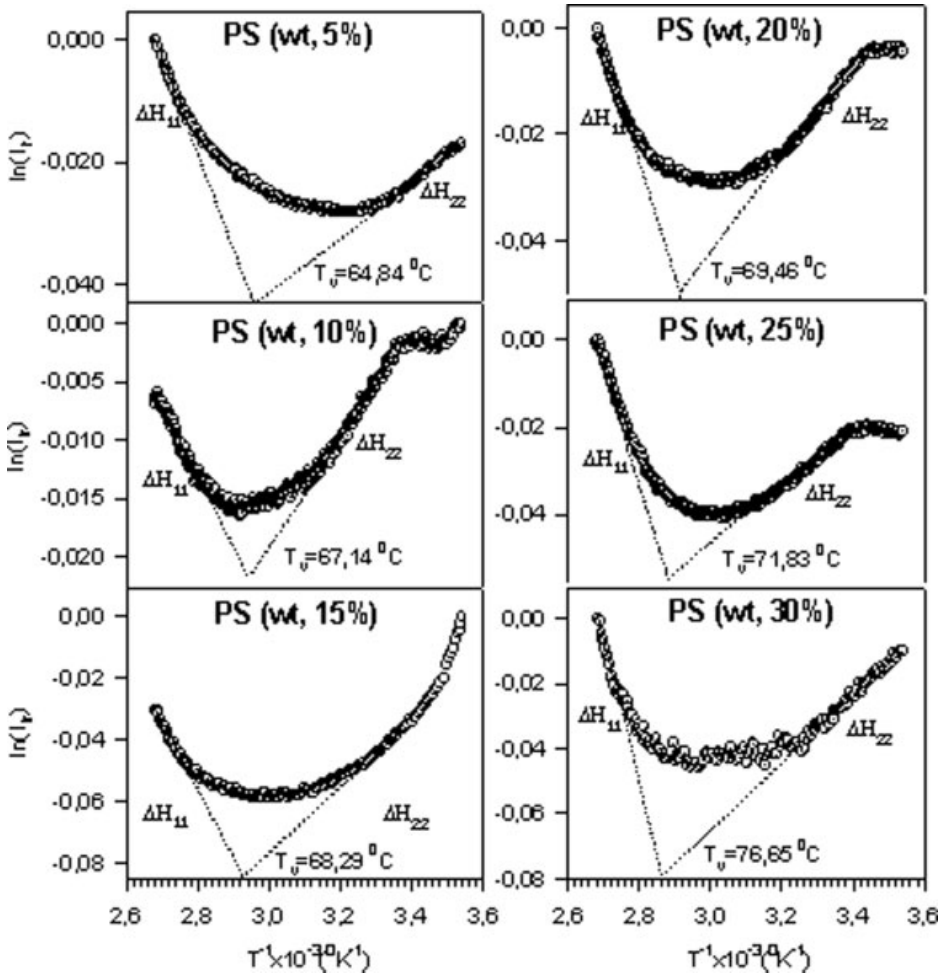


FIG. 8. Plots of ln I_{tr} versus T^{-1} curves and their fits to *Eq. 12* for cooling process. The slopes of straight lines produced void reconstruction activation energies (ΔH_{11} and ΔH_{22}).

the maxima of transmitted light intensity $(I_{tr})_m$ versus PS content are also plotted in Fig. 5, where it is seen that $(I_{tr})_m$ has decreased to very low values for all samples above 30 wt % PS content. This behavior of I_{tr} can be explained by percolating PS particles in PNIPAM lattice.

Critical Exponents

The above findings can be rationalized by first assuming that $P_\infty(p)$ is proportional to the transmitted light intensity, I_{tr}. Second assumption can be made by using the following ratio:

$$R = \frac{M_{PS}}{M_{PS} + M_{PNIPAM}} \tag{8}$$

where M_{PS} and M_{PNIPAM} present the weight of PS and PNIPAM in the film. If R is assumed to be the occupation probability, p, of PS in the PNIPAM lattice, then the percolation threshold, p_c, becomes R_c, and *Eq. 1* can be written as

$$I_{tr}(R) = (R - R_c)^\beta \tag{9}$$

Equation 9 describes the percolation model for PS distribution in PNIPAM lattice. When R approaches R_c, the largest cluster of PS appears by connecting the left and right edges to the bottom edge of the PNIPAM lattice. As PS wt % approaches to 0.30 (see Fig. 5), $(I_{tr})_m$ drops to lowest value, where $R_c = 0.30$ is very close to the site percolation value for simple cubic lattice.

In Fig. 6, log–log plot of *Eq. 9* is fitted to the data in Fig. 5, where the slope of the straight line produced the critical exponent, $\beta = 0.91$, which is in good agreement with the classical model [31].

Void Closure

In order to quantify the heating and cooling curves presented in Fig. 2, void closure model can be applied, where decrease in void size (r) causes an increase in $I_{tr}/(I_{tr})_{max}$ ratios and vice versa. If the assumption is made that $I_{tr}/(I_{tr})_{max}$ ratio is inversely proportional to the sixth power of void radius, r then *Eq. 7* can be written as

$$t = \frac{2AC}{\gamma} \exp\left(\frac{\Delta H}{kT}\right) \left(\frac{I_{tr}}{(I_{tr})_{max}}\right)^{1/3} \tag{10}$$

Here r_0^{-2} is omitted from the relation since it is very small compared to r^{-2} values after void closure processes is started. *Equation 8* can be solved for $I_{tr}/(I_{tr})_{max}$

 DOI 10.1002/pc

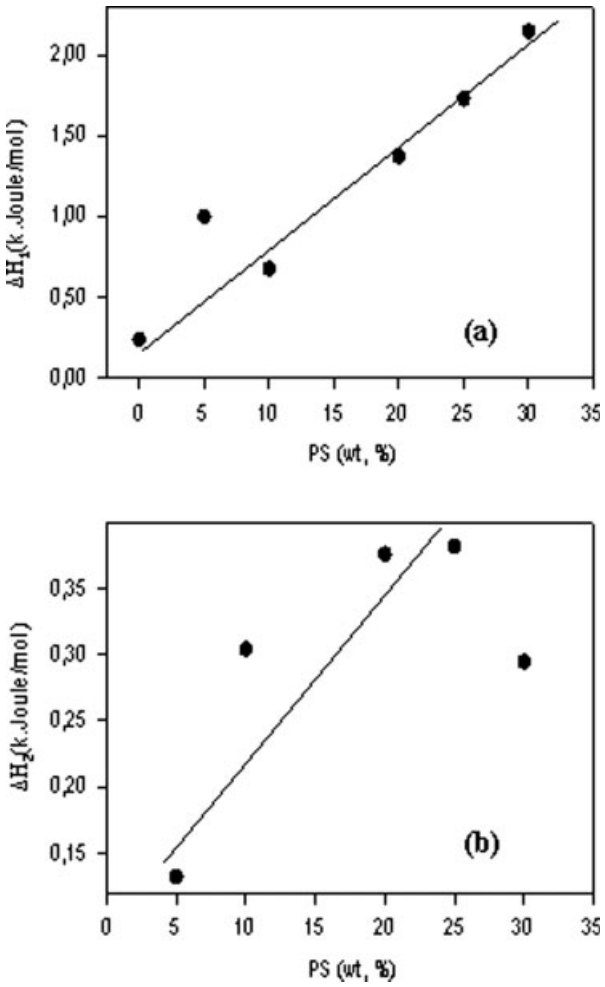


FIG. 9. Plots of void closure activation energies (a) ΔH_1 and (b) ΔH_2 against PS content.

$$I_{tr}(T) = S(t)\exp\left(-\frac{3\Delta H}{kT}\right) \tag{11}$$

where $S(t) = (yt/2AC)^3$ and $I_{tr} = I_{tr}/(I_{tr})_{max}$. For a given time the logarithmic form of *Eq. 9* can be written as follows:

$$\ln I_{tr}(T) = \ln S(t) - \left(\frac{3\Delta H}{k_B T}\right) \tag{12}$$

Equation 12 can now be used to produce ΔH activation energies. In Figures 7 and 8, ln I_{tr} versus T^{-1} plots and their fits to *Eq. 12* are presented for heating and cooling processes respectively. Here, void closure (ΔH_1 and ΔH_2) and void reconstruction (ΔH_{11} and ΔH_{22}) activation energies are produced from heating and cooling curves, respectively. The produced ΔH activation energies are plotted vs PS content for heating and cooling process in Figs. 9 and 10 respectively. It is seen that two different activation energies were observed, both for heating and cooling processes. In other words, reversible film formation in PS-doped PNIPAM particles is a two-step process. At first, system takes energy to accomplish phase separation, and then releases its energy to form a homogenous film during heating. Similarly, during cooling PS–PNIPAM system takes and gives back its energy for reversible process, ending film with voids again. It is seen in Figs. 9 and 10 that all ΔH energies increase as PS content in PNIPAM film is increased indicating that both void closure and reconstruction processes require larger energy to be accomplished when the doping material is increased. Here we have to note that I_{tr} decreases during phase separation and then increases during homogeneous film formation during heating, dividing the void closure in a two step process. During cooling, however, these processes are reversed to complete the void reconstruction process.

Careful analysis of Figs. 7 and 8 shows that increase in PS content cause a shift of the intercept (T_v) of the straight lines to higher temperatures. The observed temperatures are plotted versus PS content in Fig. 11a and b for heating and cooling process. In both cases, intercept temperature, T_v, increased as PS content is increased, predicting that higher temperature is required for film formation from doped films.

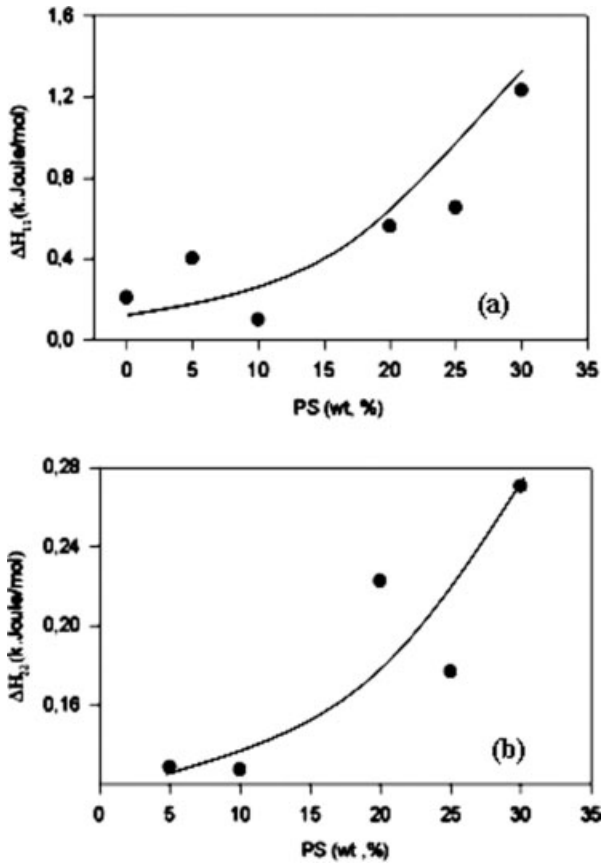


FIG. 10. Plots of void reconstruction activation energies (a) ΔH_1 and (b) ΔH_2 against PS content.

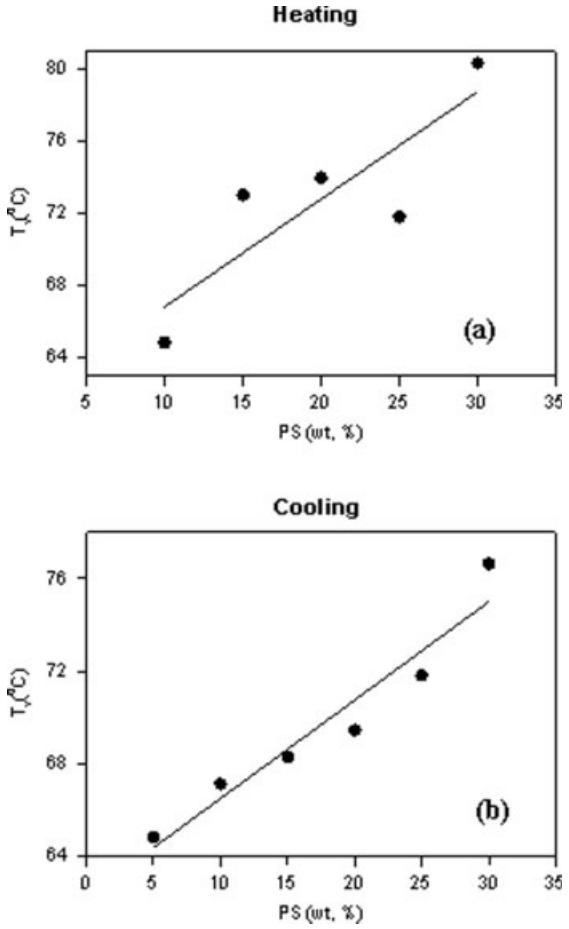


FIG. 11. Plots of intercept temperature, T_v shown in (a) Fig. 7 and (b) Fig. 8 versus PS content.

REFERENCES

1. B.R. Saunders and B. Vincent, *Adv. Colloid Interface Sci.*, **80**, 1 (1999).
2. M.J. Murry and M.J. Snowden, *Adv. Colloid Interface Sci.*, **54**, 73 (1995).
3. (a) H. Senff and W. Richtering, *J. Chem. Phys.*, **111**, 1705 (1999); (b) H. Senff and W. Richtering, *Langmir*, **15**, 102 (1999).
4. E. Bartsch, S. Kirsch, P. Lindner, T. Scherer, and S. Stolken, *Ber. Bunsen-Ges Phys Chem.*, **102**, 1597 (1998).
5. P. Branda, P. Stern, O. Quadrat, and J. Snuparek, *Colloid Polym. Sci.*, **273**, 324 (1995).
6. P.F. Kiser, G. Wilson, and D. Needham, *Nature*, **394**, 459 (1998).
7. (a) R.H. Pelton and P. Chibante, *Colloids Surf.*, **120**, 247 (l986); (b) K. Chan, R.H. Pelton, and J. Zhang, *Langmuir*, **15**, 4018 (l999); (c) J. Zhang and R.H. Pelton, *Langmuir*, **15**, 8032 (1999); (d) J. Zhang, R.H. Pelton, and Y. Deng, *Langmuir*, **II**, 2301 (1995); (e) K.C. Tam, S. Ragaram, and R.H. Pelton, *Langmuir*, **10**, 418 (1994); (f) R.H. Pelton, H.M. Pelton, A. Morfesis, and R.L. Rowell, *Langmuir*, **5**, 816 (1989).
8. S. Hirotsu, Y. Hirokawa, and T. Tanaka, *J. Chem. Phys.*, **87**, 1392 (1987).
9. C. Wu, *Polymer*, **39**, 4609 (1998); (b) C. Wu and S.Q. Zhou, *Macromolecules*, **29**, 1584 (1996); (c) C. Wu, *J. Macromol. Sci. Phys.*, **36**, 345 (1997); (d) X.H. Wang, X.P. Qiu, and C. Wu, *J. Macromolecules*, **31**, 2972 (1988).
10. L.T. Lee and B. Cabane, *Macromolecules*, **30**, 6559 (1997).
11. O.D. Kiminta, P.F. Luckham, and S. Lenon, *Polymer*, **36**, 4827 (1995).
12. M.J. Snowden, B.Z. Choudhry, B. Vincent, and G.E. Morris, *J. Chem. Soc. Faraday Trans.*, **92**, 5013 (1996).
13. T. Hellweg, C.D. Dewhurst, E. Brucker, K. Kratz, and W. Eimer, *Colloid Polym. Sci.*, **278**, 972 (2000).
14. J.D. Debord and L.A. Lyon, *J. Phys. Chem.*, **104**, 6327 (2000).
15. (a) J.M. Weissmann, H.B. Sunkara, A.S. Tse, and S.A. Asher, *Science*, **274**, 959 (1996); (b) J.H. Holtz and S.A. Asher, *Nature*, **389**, 829 (1997).
16. P.R. Sperry, B.S. Snyder, M.L. O'Dowd, and P.M. Lesko, *Langmuir*, **10**, 2619 (1994).
17. J.K. Mackenzie and R. Shuttleworth, *Proc. Phys. Soc.*, **62**, 838 (1949).
18. K.D. Kirn, L.H. Sperling, and A. Klein, *Macromolecules*, **26**, 4624 (1993).
19. O. Pekcan, M.A. Winnik, and M.D. Croucher, *Macromolecules*, **23**, 2673 (1990).
20. Y. Wang, C.L. Zhao, and M.A. Winnik, *J. Chem. Phys.*, **95**, 2143 (1991).
21. Y. Wang and M.A. Winnik, *Macromolecules*, **26**, 1347 (1993).
22. M. Canpolat and O. Pekcan, *J. Polym. Sci. Polym. Phys. Ed.*, **34**, 691 (1996).
23. O. Pekcan and E. Arda, *Encyclopedia of Surface and Colloid Science*, Marcel and Dekker, 2691 (2002).
24. O. Pekcan, E. Arda, V. Bulmus, and E. Piskin, *J. Appl. Polym. Sci.*, **77**, 866 (2000).
25. E. Arda, F. Ozer, E. Piskin, and O. Pekcan, *J. Coll. Interface Sci.*, **233**, 271 (2001).
26. E. Arda and Ö. Pekcan, *Polymer*, **42**, 7419 (2001).
27. F. Meunier, A. Elaissari, and C. Pichot, *Pol. Adv. Technol.*, **6**, 489 (1995).
28. F. Meunier and A. Elaissari, "Poly(N-Isopropylacrylamide)-Based Particles: Preparation and Colloidal Characterization," in *Surfactant Science Series*, *Vol.* **115**, Marcel Dekker, New York, 117–144 (2003).
29. S.R. Broadbent and J.M. Hammersley, *Proc. Camb. Phil. Soc.*, **53**, 629 (1957).
30. M. Sahimi, *Applications of Percolation Theory*, Taylor and Francis, London (1994).
31. D. Stauffer, *Introduction to Percolation Theory*, Taylor and Francis, London (1985).
32. J.L. Keddie, P. Meredith, R.A.L Jones, and A.M. Donald, "Film Formation in Waterborne Coatings," in *ACS Symposium Series*, *Vol.* **648**, T. Provder, M.A. Winnik, and M.W. Urban, Eds., American Chemical Society, 332–348 (1996).
33. G.B. McKenna, in *Comprehensive Polymer Science*, *Vol.* **2**, C. Booth and C. Price, Eds., Pergamon Press, Oxford, UK (1989).
34. H. Vogel, *Phys. Z.*, **22**, 645 (1925).
35. G.S. Fulcher, *J. Am. Ceram. Soc.*, **8**, 339 (1925).
36. J. Frenkel, *J. Phys. USSR*, **9**, 385 (1945).

DOI 10.1002/pc